MASTER

CONF-761012--15

TOKAMAK EXPERIMENTAL POWER REACTOR STUDIES

By

Weston M. Stacey, Jr., Charles C. Baker, Michael Roberts

Prepared for

Sixth International Conference
on Plasma Physics and Controlled Nuclear Fusion Research
Berchtesgaden, Federal Republic of Germany
October 6-13, 1976

NOTICE
This report was prepared as an account of work sponsored by the United States Government. Neither the United States nor the United States Energy Research and Development Administration, nor any of their employees, nor any of their contractors, subcontractors, or their employees, makes any warranty, express or implied, or assumes any legal liability or responsibility for the accuracy, completeness or usefulness of any information, apparatus, product or process disclosed, or represents that its use would not infringe privately owned rights.

OT W-31-109-ENG-38

UofC-AUA-USERDA

ARGONNE NATIONAL LABORATORY, ARGONNE, ILLINOIS

operated under contract W-31-109-Eng-38 for the
U. S. ENERGY RESEARCH AND DEVELOPMENT ADMINISTRATION

The facilities of Argonne National Laboratory are owned by the United States Government. Under the terms of a contract (W-31-109-Eng-38) between the U. S. Energy Research and Development Administration, Argonne Universities Association and The University of Chicago, the University employs the staff and operates the Laboratory in accordance with policies and programs formulated, approved and reviewed by the Association

MEMBERS OF ARGONNE UNIVERSITIES ASSOCIATION

The University of Arizona
Carnegie-Mellon University
Case Western Reserve University
The University of Chicago
University of Cincinnati
Illinois Institute of Technology
University of Illinois
Indiana University
Iowa State University
The University of Iowa
Kansas State University
The University of Kansas
Loyola University
Marquette University
Michigan State University
The University of Michigan
University of Minnesota
University of Missouri
Northwestern University
University of Notre Dame
The Ohio State University
Ohio University
The Pennsylvania State University
Purdue University
Saint Louis University
Southern Illinois University
The University of Texas at Austin
Washington University
Wayne State University
The University of Wisconsin

NOTICE

This report was prepared as an account of work sponsored by the United States Government. Neither the United States nor the United States Energy Research and Development Administration, nor any of their employees, nor any of their contractors, subcontractors, or their employees, makes any warranty, express or implied, or assumes any legal liability or responsibility for the accuracy, completeness or usefulness of any information, apparatus, product or process disclosed, or represents that its use would not infringe privately-owned rights. Mention of commercial products, their manufacturers, or their suppliers in this publication does not imply or connote approval or disapproval of the product by Argonne National Laboratory or the U. S. Energy Research and Development Administration

Paper for presentation at the *Sixth International Conference on Plasma Physics and Controlled Nuclear Fusion Research*, October 6-13, 1976, Berchtesgaden, Federal Republic of Germany.

Tokamak Experimental Power Reactor Studies*

Weston M. Stacey, Jr.
Argonne National Laboratory

Charles C. Baker
General Atomic Company

Michael Roberts
Oak Ridge National Laboratory

United States of America

*Work supported by the U. S. Energy Research and Development Administration and the Electric Power Research Institute (GA).

Tokamak Experimental Power Reactor Studies

Weston M. Stacey, Jr.
Argonne National Laboratory

Charles C. Baker
General Atomic Company

Michael Roberts
Oak Ridge National Laboratory

United States of America

Scoping [1-3] and conceptual design [4-6] studies for a tokamak experimental power reactor (EPR) have been conducted for the past two years at Argonne National Laboratory, General Atomic Company, and Oak Ridge National Laboratory. The purpose of these studies was to define the physics and technological features of an EPR which could operate in the mid-to-late 1980s at or near net electrical power production conditions with a plant capacity factor in the range 25-50%, thereby providing perspective on the role of the EPR in the USERDA tokamak program.

1. DESIGN DESCRIPTION

Salient features of the three designs are illustrated in Figs. 1-3. The principal geometric parameters are given in Table I. The design-basis operating parameters are given in Table II.

2. PLASMA PHYSICS

2.1 MHD Equilibrium/Stability and Performance

A range of MHD equilibrium solutions, corresponding to different pressure profiles and degrees of diamagnetism/paramagnetism, is possible for a given toroidal field and design geometry. These solutions require different equilibrium fields, of course, and have associated with them different sets of values for the plasma current, q and β_t.

Possible solutions which satisfy $q \geq 1$ for the ANL design are shown in Fig. 4. The solid curves are loci of equilibria varying (from left to right)

from highly diamagnetic to highly paramagnetic plasmas, for a given pressure profile exponent, α.* Current reversal in part of the torus occurs for solutions to the left of the dashed line. The maximum value of β_t, hence the maximum power density, occurs for equilibria slightly less diamagnetic than those for which current reversal occurs. Thus, the dashed line represents a locus of "optimal" solutions — the value of β_p along this locus is confined to a rather narrow range of $1.8 \geq \beta_p \geq 1.6$. The value of q(a) increases with the peaking of the pressure profile (i.e. with increasing α). The ANL reference design point was chosen by selecting the pressure profile for which q(a) = 3. The pressure profile, with $\alpha = 1.3$, was factored into density and temperature profiles of the same form, but with exponents $\alpha_n = 0.3$ and $\alpha_T = 1.0$, in evaluating the power balance equations.

The MHD stability of the GA Doublet configuration has been examined with respect to localized interchange modes and axisymmetric rigid displacements. Stable equilibria have been determined for high beta conditions ($\beta \geq 10\%$) with the field-shaping coils displaced sufficiently far from the plasma surface to allow for shielding. In the reference design, it was also possible to remove several coils to allow for pumping ports with no adverse effect on the equilibrium or stability. Maximum stable plasma currents and β_t are found by increasing β_p, flattening the current profile and shaping the plasma such that about 50% of the poloidal flux is inside the Doublet separatrix. The reference case assumes that $\beta_p = 1.8$ and that the on-axis current density is twice the current density at the limiter. Typical plasma current, pressure, temperature, and densities profiles are shown in Fig. 5.

In the ORNL reference design account has been taken of the unique features of the poloidal field system design. The design includes vertical field-shielding (VF-S) coils between the plasma boundary and the toroidal coils. Appropriate equilibria produced by this system have been computed for the ORNL-EPR using a free boundary MHD code.

The plasma parameters corresponding to the three reference designs are shown in Table III.

2.2 Impurity Control

The performance of the EPR with a bare stainless steel wall and no means of impurity control would be very poor. Modification of the first-wall surface, a flowing gas boundary, and a divertor were considered.

The net electrical power is plotted as a function of the length of the burn pulse, for several first-wall surface materials, in Fig. 6. Steel, niobium, and to a lesser degree, tungsten surfaces result in very poor performance because large supplemental beam heating ($P_B \approx 80$ MW) is required to offset the enhanced radiation loss due to high-Z plasma contamination. With a low-Z surface the performance is much better, except for carbon in the temperature range ~400-700°C, where chemical sputtering causes excessive plasma contamination. A low-Z material coating on a metal substrate is used for impurity control in the ANL and ORNL designs, and a low-Z standoff liner is used in the GA design.

---

*$p(r) = p_0[1 - (r/a)^2]^\alpha$

A flowing plasma boundary concept was selected for additional plasma impurity control for the GA design. Since the plasma boundary region is expected to be collisional, by modifying the impurity diffusion due to ion-impurity collisions, the inward diffusion of impurity ions can be inhibited. This is accomplished by injecting cold fuel at the top of the vacuum chamber and pumping at the limiter located at the bottom of the vacuum chamber. The required throughput is 1.6×10^{23} particles/s. The density profile which results is compatible with concepts on profile inversion for trapped particle mode stabilization and possible edge convection fueling. The flowing plasma boundary is also considered as an ash or alpha particle removal system.

2.3 Transport Scaling

A multiregime transport model is used to compute the confinement parameters. At high collision frequencies, the particle and electron energy confinement are computed from pseudoclassical theory and ion energy confinement is computed from neoclassical theory. When collision frequencies are less than bounce frequencies, the confinement parameters are computed from trapped particle (TEM, TIM) theory or pseudoclassical/neoclassical theory, whichever is least favorable. Electron energy confinement times for the GA design are plotted as a function of electron temperature in Fig. 7. Three transport scenarios are displayed. The temperature, density, and shear profiles used are characteristic of the Doublet configuration with a flowing plasma boundary for impurity control after ignition. The first scenario is essentially that documented in WASH-1295. The second and third scenarios include the effects of stabilization terms on the long wavelength trapped electron and ion modes, due to shear, Landau damping and ion-ion collisions. The third differs from the second by the inclusion of various short wavelength trapped electron residual modes, and is the transport model adopted for use in the GA design.

2.4 Burn Cycle Dynamics

The basic burn cycle is illustrated schematically in Fig. 8 (times are representative of the ANL design). As the plasma current rises, the equilibrium field must increase to provide MHD equilibrium. The beam heating may be initiated during or after the ohmic heating current ramp.

The requirements on the plasma driving and heating systems are quite sensitive to the startup procedure. The energy transferred in the ohmic heating system (U_{OH}), the energy transferred into the neutral beam injection system (U_{BE}), the maximum field (B_{OH}) and field rise ($\dot{B}_{OH}$) in the ohmic heating coils, and the maximum power (P_{EF}) transferred by the equilibrium field power supply are plotted in Fig. 9 versus the ohmic heating current reversal time (Δt_{OH}), for the ANL design. By starting up with the maximum plasma current (subject to q and ion sound speed limitations), the required plasma auxiliary heating power is minimized, as illustrated in Fig. 10 for the GA design. The disadvantage is that additional volt seconds are used during startup. The maximum plasma heating power (and energy) results when startup is accomplished at the maximum allowed β_p. As a result of studies of this type, the requirements shown in Table IV were identified.

Reference case power performance characteristics for the three designs are summarized in Table V. Supplemental beam heating can be provided to achieve this level of energy output even if the energy confinement is inadequate for ignition; however, it would be difficult to achieve net power in

this case. Supplemental beam heating can also be used to achieve longer burn cycles by maintaining thermonuclear temperatures against the accumulation of wall-sputtered impurity and helium. It is assumed that the D-T ion density can be maintained during the burn by a combination of recycling and refueling; however, burn pulses up to 30-45 s may be possible without refueling, if recycling is effective. The average net electrical power for the ANL design is shown in Fig. 11 as a function of the length of the burn pulse.

3. TECHNOLOGY

3.1 First-Wall System

A first-wall system which can maintain its structural integrity under the thermal, stress, and radiation conditions imposed by the size of the vacuum chamber and the pulsed mode of operation is one of the more demanding technological requirements for the EPR. The three designs are summarized in Table VI, and the performance characteristics are given in Table VII.

The ANL design consists of a self-supporting vacuum chamber wall consisting of 16 segments, with rib-and-spar support and detachable coolant panels mounted on the inside. The vacuum vessel supports the pressure differential and gravitational loads, while the coolant panels absorb the most severe thermal loads but perform no structural function. The coolant panels are coated on the plasma side with 100-200 microns of beryllium for impurity control.

The GA first wall is formed by disk-shaped silicon-carbide liner plates, which are attached to each blanket module and cooled by thermal radiation to the blanket modules. The vacuum chamber is formed by the modules and seal rings welded between the modules and the support frame.

In the ORNL design, an independently cooled, 1-cm thick vacuum vessel segment is mounted on the inside of each blanket segment. This vacuum vessel is a composite Type 316 stainless steel structure with a honeycomb interior enclosed between two 0.16-cm thick plates. Water enters at approximately 100°F and exits at about 250°F at 50 psi pressure. The wall is divided poloidally into 4 quadrants, and with 60 blanket segments there are 240 first-wall "quadrants". Between blanket segments, the wall segments are welded by bellows closures to form a vacuum chamber.

3.2 Blanket/Shield Systems

The blanket/shield system consists of the blanket, the bulk shield, and special penetration shields for the neutral beam lines, vacuum ducts, etc. The thickness of the blanket is chosen such that most of tthe fusion energy is deposited therein, and the thickness of the bulk shield is determined by magnet protection criteria. There is incentive to minimize the shield thickness on the inside of the torus in order to maximize the toroidal field in the plasma. Features of the three designs are summarized in Table VIII.

The blanket in the ANL design consists of 0.28-m thick stainless steel blocks, with drilled 1-cm diameter coolant passages, surrounding the first wall assembly. The bulk shield surrounds the blanket, varying in thickness from 0.58-cm on the inside of the torus, where highly radiation-attenuating material is used, to 0.97 m on the outside of the torus. A shield plug blocks the penetration formed by the vacuum duct during the plasma burn. Special,

highly attenuating SS/B_4C shields surround the neutral beam lines after they exit from the bulk shield until they pass the TF coils. A blanket similar to that surrounding the vacuum vessel surrounds the beam penetrations through the bulk shield. The blanket and shield are segmented into 688 electrically insulated blocks to inhibit the development of eddy currents which would distort the penetration of the equilibrium field. The blanket and bulk shield are cooled by H_2O at 2000 psi and atmospheric pressure, respectively.

The main body of the GA blanket, that portion in which fusion neutrons are intercepted and the thermal energy is deposited, is comprised of 1900 cylindrical blanket modules which mount onto the support structure. These 42-cm diameter by 25-cm long modules are fabricated from 20% CW Type 316 stainless steel and incorporate radial coolant holes near the front face with axial coolant passages through the interior. After passing through coolant channels in the module support ring, the 4.9 MPa helium coolant, which enters at 325°C, flows axially towards the blanket wall through coolant holes along the module circumference. The full helium flow is thereby delivered, while it is still relatively cool, to the blanket wall where the heating rates are most severe. The coolant flows radially along the blanket wall, then axially through the module interior in annular passages formed by holes with rod inserts and finally into a plenum and out of the module at 575°C. Metal temperatures do not exceed 600°C, and thermal stresses are maintained within allowable limits by selection of appropriate coolant passage size and spacing. The spaces between modules in the blanket are filled with permanent graphite blocks and graphite rings, which are removable for module maintenance. These graphite sections are cooled by radiation to the blanket modules and reach a maximum temperature of about 1600°C.

Each of the 60 blanket segments in the ORNL design has been divided poloidally into 12 modules. Each module consists of (1) a helium-cooled liquid metal (potassium or lithium region; (2) a graphite reflector; and (3) stainless steel region. The modular division reduces coolant pressure drop by simplifying the coolant pumping. By breaking the segments into modules, eddy currents are reduced in the lithium also.

3.3 Plasma Heating

Current experience dictates that neutral beam injection be the reference option for plasma heating. The injection heating requirements are indicated in Table IV. The ANL and GA designs are based upon positive ion sources, while the ORNL design is based upon a negative ion source.

Four neutral beam injector systems capable of injecting 60 MW of 180 keV D^0 into the plasma for the ANL design are compared in Table IX. Design 1 is based upon modest extrapolations beyond present results with D^+ sources, design 2 is based upon an improved D^+ source, and designs 3 and 4, which would require considerable advance in source technology, are based upon direct-extraction D^- sources. All designs introduce large ($\sim$1/2 to 1 m^2) penetrations in the shield for neutron and gamma streaming, and design 1 has very demanding vacuum system requirements. Substantial improvements in power efficiency and corresponding reductions in power requirements and gas loads can be realized if D^+ sources with a very high atomic component are developed, and even more dramatic improvements are promised by direct extraction D^- sources.

Radio-frequency heating is an attractive alternative to neutral beam heating, from the technological point of view. Efficient power sources exist for lower hybrid and ion cyclotron heating. The neutron streaming problem is less severe than with neutral beam injectors, where a straight-line penetration of the shield is intrinsic.

3.4 Toroidal Field Coils

The relatively long burn pulse dictates that the toroidal field coils be superconducting. ANL and GA chose niobium-titanium as the superconductor, because of its good ductility and proven performance in large magnets, while ORNL uses Nb_3Sn on the inside leg, to achieve high fields, and niobium-titanium elsewhere. The TF coil designs are summarized in Table X.

Superimposed pulsed fields from the poloidal coils and the plasma are one of the most difficult problems in the TF coil design. ANL employed an aluminum shield operating at 18°K to shield the TF conductor from the ac heating and out-of-plane load due to the pulsed field. In the GA design, the field-shaping coil system, which is located internal to the TF coils near the plasma, significantly reduces the superimposed pulsed fields in the region of the TF coils. The ORNL design employs an electromagnetic shielding system to resolve this problem.

Unequal currents in the TF coils could create large forces and torques between coils and large bending moments in each coil, which could produce severe damage. The ANL and GA designs are protected against this possibility by series operation, with quench protection provided by discharging the TF coils through large resistors that are activated by switches. In the ORNL design, the TF coils are connected in several parallel loops, with the objective of being able to isolate and discharge only quenched coils.

3.5 Poloidal Field Coils

The poloidal coil system consists of the ohmic-heating (OH) coils, the equilibrium field (EF) or field-shaping coils, and additional coils for plasma initiation and control. The poloidal coil systems designs are summarized in Table XI.

In the ANL design, both the OH and EF coils are superconducting and are located external to the TF coils. The OH and EF coil problems are similar — large stored energy, high operational current, rapid charging and discharging and ring coil configuration. A set of water-cooled copper coils is located inside the TF coils near the plasma and is used to provide ∿500 V for plasma initiation and for equilbrium field trimming.

The GA design uses superconducting OH coils located external to the TF coils and oil-cooled, copper field-shaping coils located internal to the TF coils near the plasma. The field-shaping coils are pulsed at 30 kV to initiate the plasma.

In the ORNL design, the OH coils are superconducting and located external to the toroidal field coils. The EF coils are located both external and internal to the TF coils. The externally located EF coils are superconducting. Those located internally are normal (copper) coils. Their function is to reduce stored energy requirements, enhance the volt-second capability of

the device, and to reduce the $\dot{B}$ experienced by the TF coils during the current rise phase of operation. The overall reduction in $\dot{B}$ is about a factor of 5.

3.6 Energy Storage and Transfer

In order to operate the poloidal coil and neutral beam systems, gigajoules of energy must be transferred in times on the order of seconds. It will be necessary to store energy on site so that the large power pulses required to initiate and terminate the plasma burn do not perturb the electrical power network.

The energy storage and transfer system for the ANL design consists of a central energy storage inductor (ESI), rectifiers to transfer energy between the ESI and the OH, EF, and neutral beam systems and a rectifier to transfer energy from a substation into the ESI. A separate inertial energy storage unit, consisting of radially stacked homopolar generators, is incorporated in the OH system, so that inductive energy is transferred between the OH coils and the homopolars, with the central ESI making up losses. Electrical energy is recovered directly in the neutral beam system. This energy storage and transfer system is summarized in Table XII.

The system employed in the GA design utilizes three large homopolar motor-generator units, each with a capacity of about 500 MJ, which provide storage for dumping the OH coils and re-energizing them during the flux swing. A conventional type motor-generator with a storage capacity of 800 MJ is provided to store the energy required by the pulse mode operation of the neutral beam injectors. This motor-generator is sized so as to accommodate the excess output when the field-shaping coils are de-energized, thereby leveling the plant output. In addition, a capacitor bank with a storage capacity of 400 MJ supplies an energy pulse to the field-shaping coils, thereby providing the volt-seconds required for initial breakdown of the plasma.

3.7 Tritium Fuel Cycle

The tritium handling system removes nonmetallic elements and other debris from the spent fuel and enriches, stores, and delivers the tritium. Operating parameters for the tritium-handling systems are given in Table XIII. The fuel cycle turnaround time is determined mainly by the regeneration cycle on the cryosorption pumping system for the toroidal vacuum chamber, and minimization of this time is crucial to minimization of the tritium inventory.

3.8 Radiation Damage

Radiation damage is an important consideration in the design of the EPR. The useful lifetime of the first-wall and innermost portions of the blanket is set by radiation damage criteria and erosion rates of the low-Z liners. Shielding requirements are determined largely by radiation protection criteria for the superconducting TF coils. A summary of radiation damage data at the design lifetime is presented in Table XIV.

3.9 Costs

Cost estimates for the ANL and GA designs are given in Table XV.

4. CONCLUSIONS

An EPR operating at or near net electrical power conditions with a capacity factor of 25-50% requires an extrapolation of plasma conditions (confinement, pulse length, etc.) beyond those anticipated for the most advanced experiments (PLT, T-10, D-III, PDX, etc.) that will be operational in the next few years. Advances beyond the current state-of-the-art in certain essential areas of fusion reactor technology (superconducting magnets, energy storage and transfer, neutral injectors, tritium, first-wall, etc.) are also required. Such an EPR represents a significant national investment. To achieve an EPR with these characteristics by the mid-to-late 1980s would be a bold stroke which would go far towards enabling a demonstration of commercial feasibility of fusion power by the end of the century. However, such an undertaking would require significant increases in technology development and EPR design effort as well as an acceleration of the tokamak experimental program, thus an increase in the funding level of the U. S. fusion program. Moreover, major design decisions would have to be made on the basis of physics information which will become available in the next few years, prior to the operation of the Tokamak Fusion Test Reactor (TFTR) and probably prior to the time at which Doublet-III and PDX reach their ultimate design goals. In addition, several advanced technologies would have to be first demonstrated in a fusion reactor environment in EPR. These factors have led to a consideration of alternatives. At the moment, it appears likely that a less ambitious device which can achieve many of the EPR objectives may be built in the mid-to-late 1980s, and that the EPR may be deferred until the early 1990s.

ACKNOWLEDGMENT

The work reported in this paper was performed by the EPR design teams at ANL, GA, and ORNL. The work was supported by USERDA and, in the case of GA, by the Electric Power Research Institute.

REFERENCES

[1] STACEY, W.M., Jr., et al., Tokamak Experimental Power Reactor Studies, Argonne National Laboratory Rep. ANL/CTR-75-2 (1975).

[2] GAC FUSION ENGINEERING STAFF, Experimental Power Reactor Conceptual Design Study — 12-Month Progress Report for the Period July 1, 1974 through June 30, 1975, General Atomic Company Rep. GA-A13534 (1975).

[3] ROBERTS, M., BETTIS, E.S., Oak Ridge Tokamak Experimental Power Reactor Study Reference Design, Oak Ridge National Laboratory Rep. ORNL/TM-5042 (1975).

[4] STACEY, W.M., Jr., et al., Tokamak Experimental Power Reactor Conceptual Design, Argonne National Laboratory Rep. ANL/CTR-76-3 (1976).

[5] BAKER, C.C., et al., Experimental Power Reactor Conceptual Design Study — Final Report for the Period July 1, 1974 through June 30, 1976, General Atomic Company Rep. GA-A14000 (1976).

[6] ROBERTS, M., Oak Ridge Tokamak Experimental Power Reactor Studies — 1976, Oak Ridge National Laboratory Rep. ORNL-TM-5572 (1976).

TABLE I. EPR GEOMETRICAL PARAMETERS

	ANL	GA	ORNL
Major radius (m)	6.25	4.50	6.75
Plasma minor radius (m)	2.10	1.12	2.25
Plasma elongation	1	3	1
First-wall minor radius (m)	2.40	1.22	2.25
Blanket thickness (m)	0.28	0.25	0.52
Shield thickness (m)			
inside	0.58	0.40	0.48
outside	0.97	1.00	0.48
Toroidal field coil bore (m)	7.8 × 12.6	8.1 × 12.4	7.4 × 9.7

TABLE II. DESIGN-BASIS OPERATING PARAMETERS

	ANL	GA	ORNL
Duty cycle (%)	75	84	87
Capacity factor = duty cycle × plant availability	50	20	70
Lifetime (yr)	10	10	10

TABLE III. STEADY-STATE PLASMA PARAMETERS

	ANL	GA	ORNL
Average total beta, β_t	0.048	0.10	0.03
Safety factor, q(a)	3.05	2.5	2.5
Plasma current, I (MA)	7.6	11.4	7.2
Average D-T temperature, $\bar{T}_{DT}$	9.6	11.4	12.6
Average D-T ion density, $\bar{n}_{DT}$ (m^{-3})	9.4×10^{19}	1.1×10^{20}	7.0×10^{19}
Effective ion charge, Z_{eff}	1.3	2.0	1.3
Energy confinement, $n\tau_E$ (s/m^3)	2.4×10^{20}	2.7×10^{20}	2.7×10^{20}
Power, P_T [MW(th)]	638	410	410

TABLE IV. PLASMA DRIVING AND HEATING SYSTEM REQUIREMENTS

	ANL	GA	ORNL
Ohmic Heating Coil System			
Volt seconds to plasma (V-s)	85	75	110
Maximum power (MW)	1900	2250	2100
Energy transferred (MJ)	1200	1300	1800
Minimum current reversal time (s)	2.0	2.0	2.0
Maximum field in conductor (T)	5.0	5.7	7.2
Maximum field rise (T/s)	6.7	9.6	7.2
Equilibrium Field Coil System[a,b]			
Volt-seconds to plasma (V-s)	50	15	55
Maximum power (MW)	420	117	126
Energy transferred (MJ)	1500	75	76
Neutral Beam Injection System			
Deuteron energy (keV)	180	125	200
Power to plasma (MW)	60	60	50
Energy to plasma (MJ)	300	120	250
Energy to injector (MJ)	1000	800	500

[a]Field-shaping coil in GA design.

[b]Two coil magnetic system in ORNL design.

TABLE V. REFERENCE BURN CYCLE POWER PERFORMANCE

	ANL	GA	ORNL
Burn pulse length (s)	55	105	100
Downtime between pulses (s)	15	20	15
Energy through first wall (GJ)	16	42	41
Thermal conversion efficiency (%)	30	41	24
Gross electrical power (MW)	72	124	99
Net electrical power (MW)	30	37	7

TABLE VI. FIRST-WALL SYSTEM DESIGN

ANL	GA	ORNL
• Free-standing, 2-cm thick 316 SS vacuum wall with rib and spar support.	• Detachable, 1-cm thick SiC liner plate disks centrally supported by bolting to blanket modules.	• Four 90-deg welded segments, 1-cm thick 316 SS, honeycomb interior.
• Detachable, 2-cm thick 316 SS coolant panels.	• Cooled by thermal radiation to face of blanket modules.	• H_2O coolant at 50 psi; separate first-wall coolant system.
• 100-200 μm beryllium coating on plasma side.	• Graphite filler blocks between modules directly exposed to plasma, cooled by thermal radiation.	• Low-Z coating on plasma side.
• H_2O coolant at 2000 psi; separate first-wall coolant system.		

TABLE VII. FIRST-WALL SYSTEM PERFORMANCE

	ANL	GA	ORNL
Vacuum Wall[a]			
Surface heat flux (MW/m^2)	0.0	0.27	0.27
Heat deposition (W/cm^3)	5.8	9.7	10.1
Maximum temperature (°C)	<500	600	125
Maximum ΔT during burn (°C)		60	20
Limiting criterion	ductility[b]	thermal fatigue	ductility[c]
Coolant Panel/Stand-off Liner			
Surface heat flux (MW/m^2)	0.13	0.17	NONE
Heat deposition (W/cm^3)	5.8	10.0	
Maximum temperature (°C)	380	1450	
Burn cycle ΔT (°C)	100	120	
Burn cycle thermal strain (%)	0.09	0.001[e]	
Limiting criterion	thermal fatigue[d]	erosion	

[a]Innermost part of blanket in GA design.

[b]1% at 2.5 $MW\text{-}yr/m^2$.

[c]Unknown, $\sim$10 $MW\text{-}yr/m^2$.

[d]5×10^6 burn cycles.

[e]Due to nonlinear temperature distribution in free-standing liner.

TABLE VIII. BLANKET/SHIELD SYSTEM

	ANL	GA	ORNL
Blanket			
Material	316 SS	316 SS	316 SS/C/K
Thickness (m)	0.28	0.25	0.52
Coolant	H_2O	He	He
Maximum temperature in structure (°C)	500	600	536
Maximum heat deposition (W/cm^3)	3.5	9.7	8.4
Bulk Shield			
Material			
inside	SS/B_4C	SS/LiH	B-H_2O/SS/Pb
outside	SS/Pb-mortar/C/Al	B_4C/Pb	B-H_2O/SS/Pb
Thickness (m)			
inside	0.58	0.40	0.48
outside	0.97	1.00	0.48
Fraction of fusion power deposited	0.07	0.01	0.07
Maximum temperature (°C)	90	165	82
Coolant	H_2O	H_2O	H_2O

TABLE IX. COMPARISON OF NEUTRAL BEAM INJECTION SYSTEMS FOR ANL DESIGN[a]

	Design 1	Design 2	Design 3	Design 4
Atomic ion	D^+	D^+	D^-	D^-
Target for $D^+ \rightarrow D^0$	D_2 gas	D_2 gas	D_2 gas	Li plasma
Beam composition (D^+, D_2^+, D_3^+/D^-)	(0.75, 0.18, 0.07/-)	(0.05, 0.03, 0.02/-)	(-/0.95)	(-/0.95)
Ion beam power (MW)	441	338	113	81
No. injectors	12	12	6	6
Gas load/injector (torr-litre)	110	57	41	11
Cryosorption panel area/injector (m^2)	100	80	45	42
Power efficiency	0.34	0.45	0.66	0.77
Net power required (MW)	207	145	91	78

[a]All four systems inject 60 MW of 180 keV D^0 into the plasma.

TABLE X. TOROIDAL FIELD COIL SYSTEM

	ANL	GA	ORNL
Superconductor	NbTi	NbTi	$NbTi/Nb_3Sn$
Coil shape	pure-tension D	pure-tension D	minimum-bending oval
No. of coils	16	16	20
Maximum field ripple (%)	1.3	<0.1	2.2
Maximum field (T)	10.0	7.9	11.0
Field at plasma center (T)	4.5	3.9	4.8
Operating temperature (°K)	3.0	4.2	4.0
Stability	cryostatic	cryostatic	cryostatic
Temperature allowance (°K)	0.5	0.8	2/5[a]
Conductor	monolithic	monolithic	cable
Ampere-turns (MAT)	134	89	162
Average current density (A/cm^2)	1463	2039	1790
Cooling	pool boiling	pool boiling	force flow
Stored energy (GJ)	30	16.7	29
Refrigeration power (MW)	14.3	3.6	12.7

[a] 2°K for NbTi/5°K for Nb_3Sn; 12°K instantaneous rise.

TABLE XI. POLOIDAL FIELD COIL SYSTEM

	OH Coil			EF Coil			
						ORNL[b]	
	ANL	GA	ORNL	ANL	GA[a]	Shield-EF	Trim-EF
Type	S/C (NbTi)	S/C (NbTi)	S/C (NbTi)	S/C (NbTi)	Cu	Cu	S/C (NbTi)
Coil design	single layer	single layer	pancake	single layer	multilayer	single turn	multilayer
Conductor	cable	cable	cable in conduit	cable	bar	monolithic	cable in conduit
Cooling	He pool boil	He pool boil	He force flow	He pool boil	oil	H_2O	He force flow
Average current density (A/cm^2)	2640	3300	1460	2946	454		
Ampere-turns (MAT)	67	71	61	±18.6	-11.6	7.2	0 (net)
Maximum operational current (kA)	80	450	100	80	75	450	400
Power supply voltage (kV)	48	10	35	21	31[c]		

[a] Field-shaping coil.

[b] Two-coil magnetic system.

[c] For plasma breakdown.

TABLE XII. ENERGY TRANSFER AND STORAGE SYSTEMS — MAXIMUM RATINGS — ANL DESIGN

Ohmic Heating Systems	
Drum homopolar generators	
No. of generators in series	16
No. of drums/generator	6
Total energy transfer (MJ)	1200
Peak power (MW)	1900
Peak voltage (kV)	51
Peak current (kA)	68
Equivalent capacitance (F)	0.897
Rectifier system	
Type	Inductor-converter bridge
Energy transfer (MJ)	600
Peak power (MW)	66
Peak current (kA)	80
Peak voltage (kV)	0.8
Equilibrium Field System	
Type	Inductor-converter bridge
Energy transfer (MJ)	1500
Peak power (MW)	416
Peak current (kA)	80
Peak voltage (kV)	21
Peak switching frequency (Hz)	1330
Neutral Beam System[a,b] (60 MW)	
Type	SCR, DC/AC/DC at 10 kHz
Energy transfer (GJ)	1
Voltage (kV)	180
Power (MW)	207
RF System (60 MW)[b]	
Type	5 phase inductor-converter bridge
Voltage (kV)	
ICR	18
LHR	64.5
Power (MW)	
ICR	94
LHR	125
Central Energy Storage Inductor	
Type	Superconductive ring dipole inductor
Energy stored (GJ)	3.2
Energy transfer (GJ)	2.4
Peak current (kA)	80
Peak power (MW)	620
Average power from 60 Hz line (MW)	21

[a]Assumes electrical energy recovery in power supply.

[b]Neutral beam and rf are alternative options.

TABLE XIII. TRITIUM FUEL CYCLE

	ANL	GA	ORNL
Burnup (g/day)	64	53	58
Throughput/burnup ratio[a]	50	270	17
Tritium delivery rate (g/hr)	150	600	41
Fuel cycle turnaround time (hr)	4	4	
Plant inventory (kg)	1.5	4.1	5-10
Annual tritium consumption (kG)	16	3.9	18
Enrichment	cryogenic distillation	cryogenic distillation	cryogenic distillation

[a]Design basis value for sizing tritium system.

TABLE XIV. RADIATION DAMAGE AT DESIGN LIFETIME

	ANL	GA	ORNL
Design lifetime integrated neutron wall load (MW-yr/m^2)	2.5	1.4	10.0
First Wall[a]			
Neutron fluence (n/cm^2)	6×10^{22}	4×10^{22}	1×10^{23}
Yield strength (ksi)[b]	75	29	110
Uniform elongation (%)	>1	nil	>4
Radiation swelling (%)	<4	2	<6
Neutron damage (dpa)	28		110
Helium generation (appm)	540	2100	1290
Hydrogen generation (appm)	1330	740	4240
Blanket			
Maximum neutron fluence (n/cm^2)	5×10^{22}	4×10^{22}	7×10^{22}
Minimum yield strength (ksi)	20	40	60
Minimum ductility (%)	>3	1	1
Maximum radiation swelling (%)	<2	0.3	<2
Maximum neutron damage (dpa)	17	22	10
Maximum helium generation (appm)	230	240	40
Maximum hydrogen generation (appm)	600	500	150
Toroidal Field Coil[c]			
Neutron fluence (n/cm^2)	4×10^{17}	1×10^{18}	2×10^{19}
Neutron damage to Cu stabilizers[d] (dpa)	8×10^{-5}	3×10^{-4}	4×10^{-3}
Radiation dose to insulator (rad)	4×10^{8}	1×10^{9}	2×10^{9}

[a]SiC liner in GA design.

[b]Ultimate.

[c]Maximum values.

[d]Without annealing.

TABLE XV. PLANT CAPITAL INVESTMENT DIRECT COST ESTIMATES ($M)

a. ANL	
Structure and site facilities	67.3
Reactor	248.6
Reactor plant facilities	245.0
Auxiliaries	18.0
TOTAL	578.9
Engineering (25%)	144.7
Contingency (25%)	144.7
GRAND TOTAL	868.3

b. GA	
Fusion steam supply system	
Equipment	179.3
Installation	37.4
Engineering	58.5
Indirects	76.3
Contingency	64.5
FSSS TOTAL	416.0
Balance of plant	279.9
GRAND TOTAL	695.9

LIST OF FIGURES

1. Vertical section of ANL EPR.

2. Vertical section of GA EPR.

3. Vertical section of ORNL EPR.

4. MHD equilibria at $B_{max}^{TFC} = 10$ T — average total beta.

5. Distributions of plasma current density, pressure, temperature, and ion density in the GA design.

6. Effect of first-wall surface material on power performance — ANL design.

7. Energy confinement time as a function of temperature for the GA design.

8. Burn cycle scenario.

9. Effect of OH current reversal time on plasma driving and heating system requirements for the ANL design.

10. Auxiliary heating power requirements for the GA design.

11. Power performance as a function of operating mode for the ANL design.

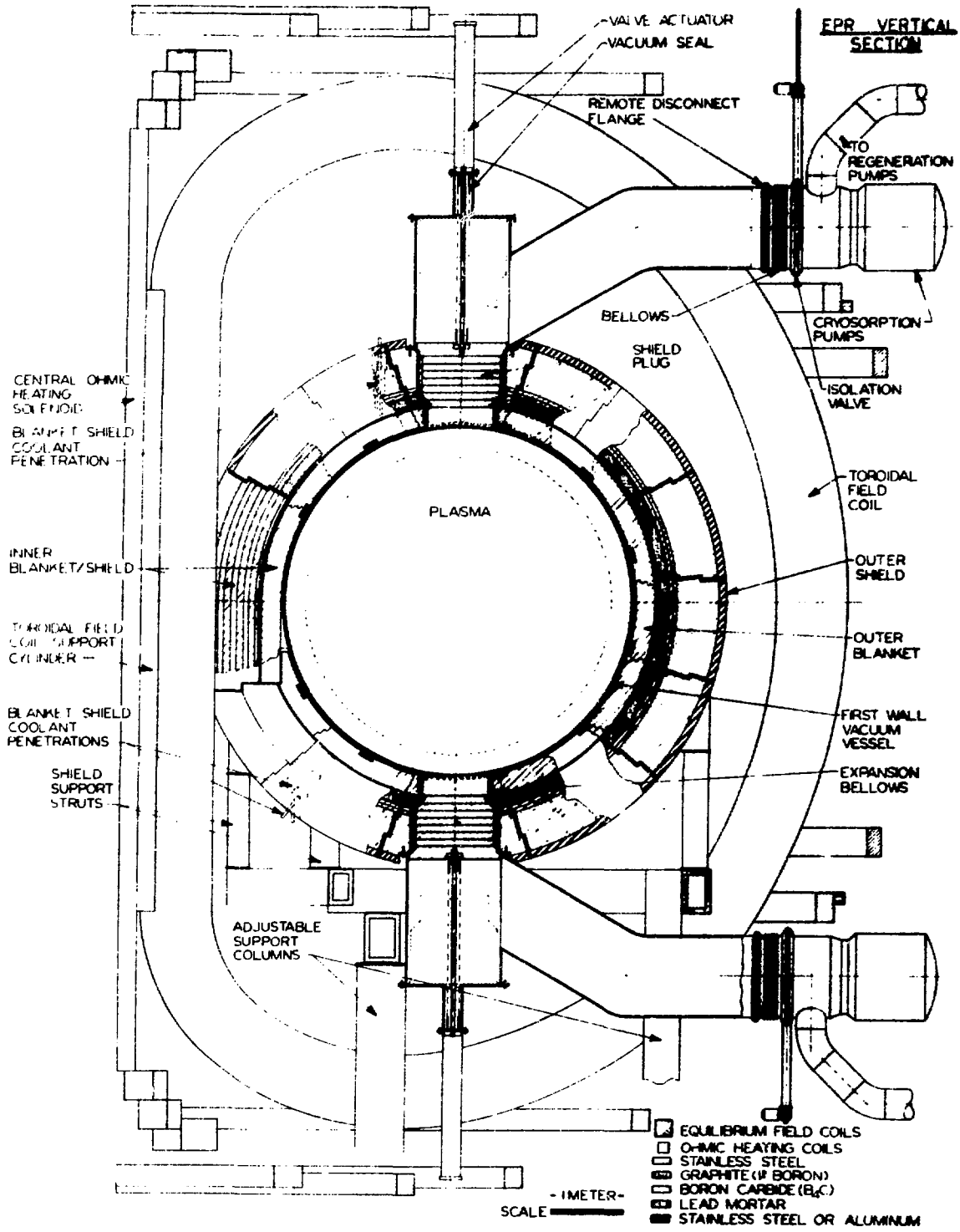

Fig. 1. Vertical section of ANL EPR.

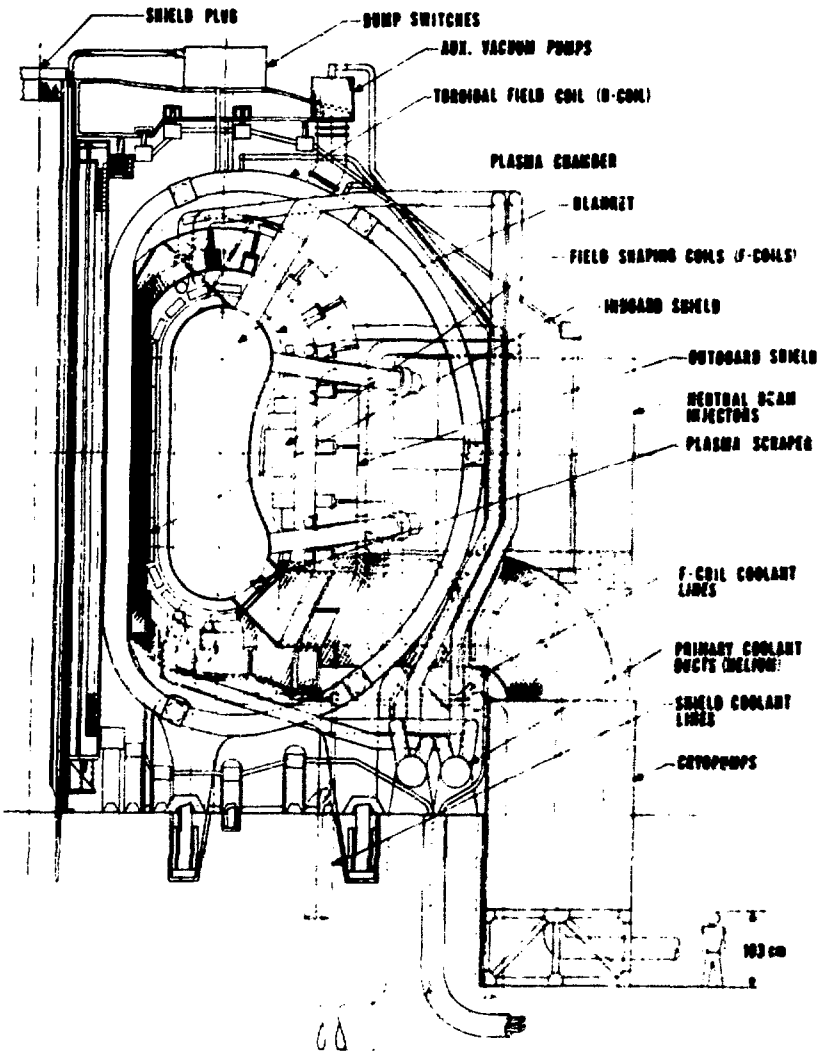

Fig. 2. Vertical section of GA EPR.

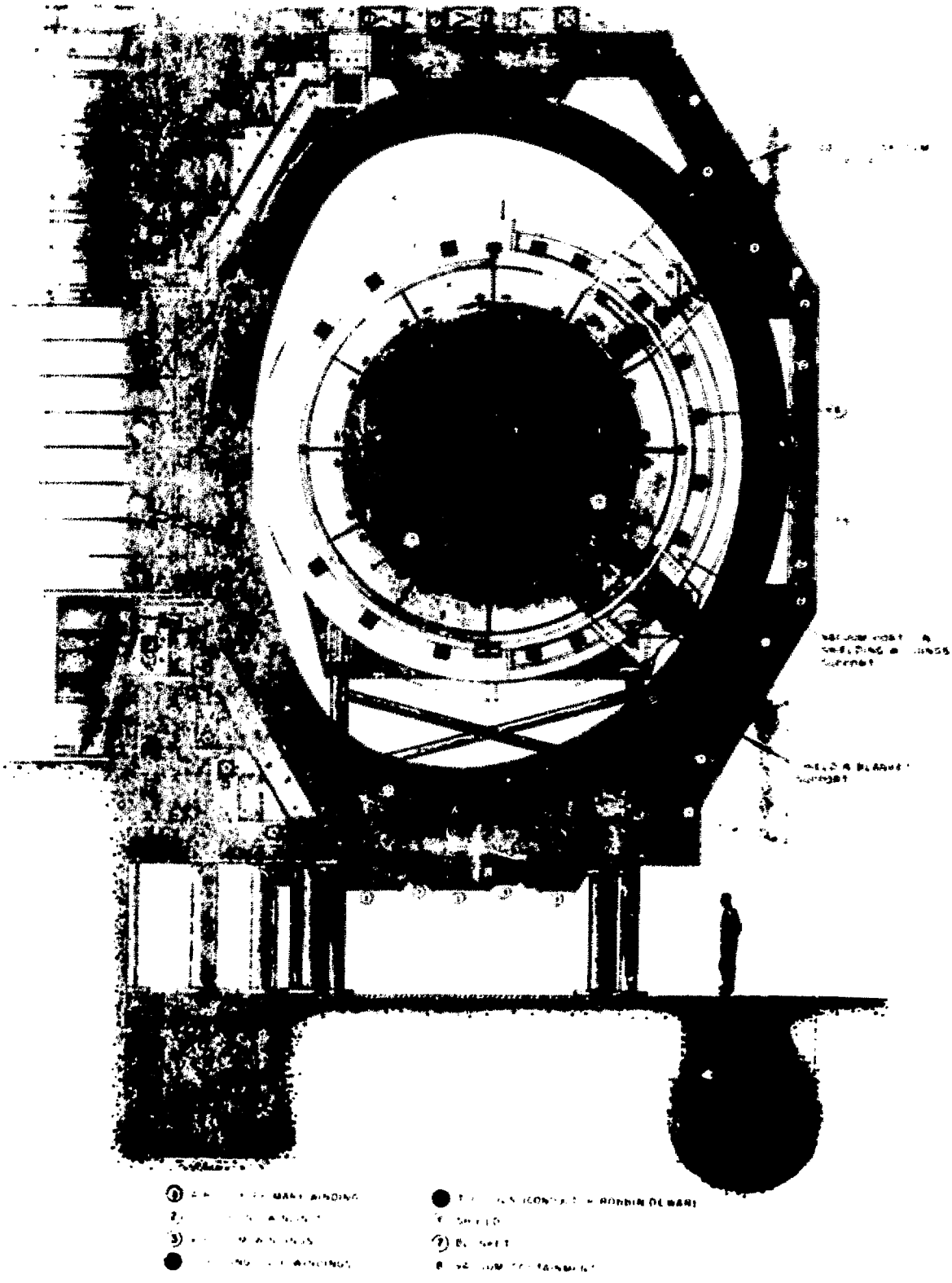

Fig. 3. Vertical section of ORNL EPR.

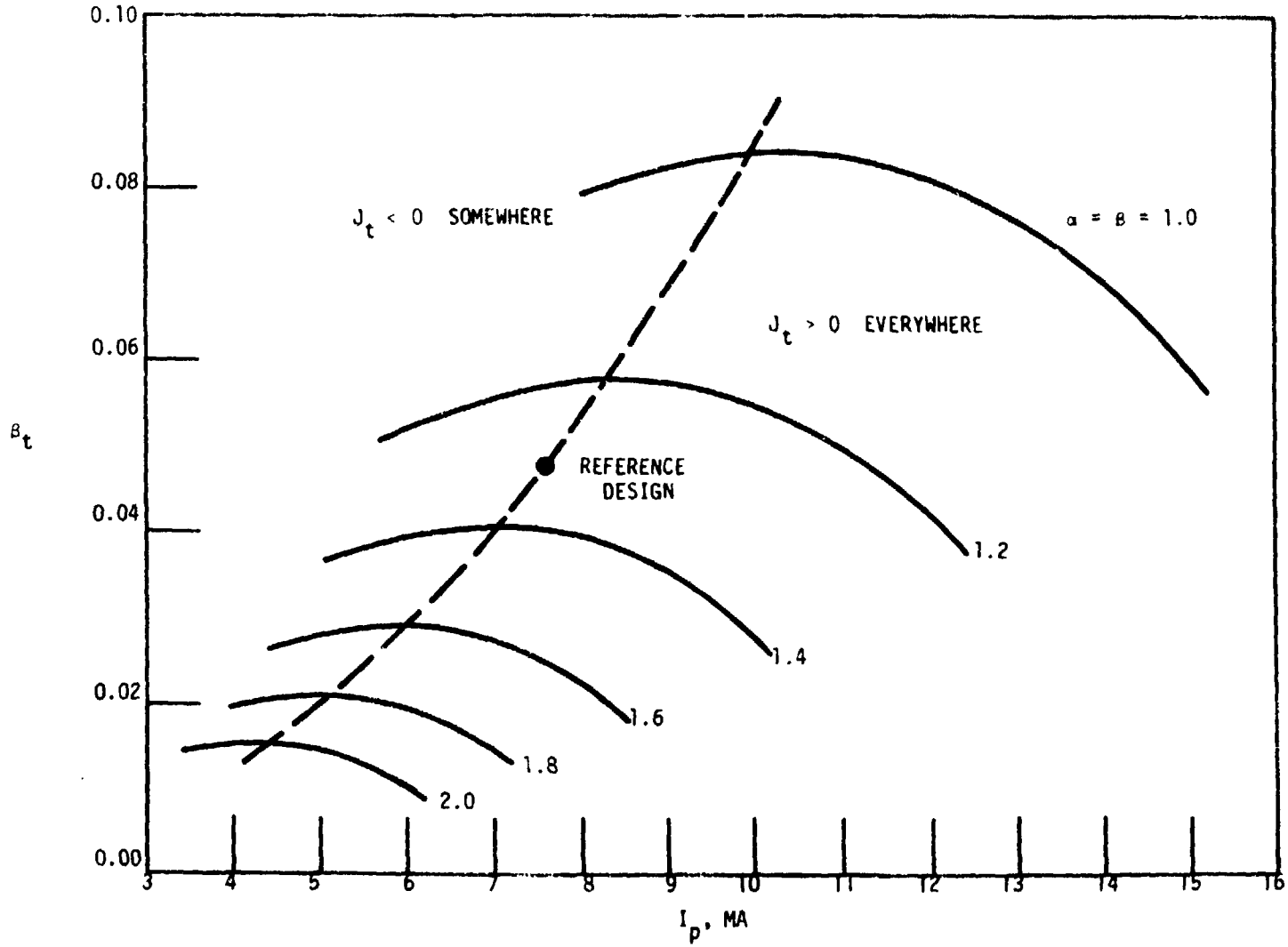

Fig. 4. MHD equilibria at $B_{max}^{TFC} = 10$ T — average beta.

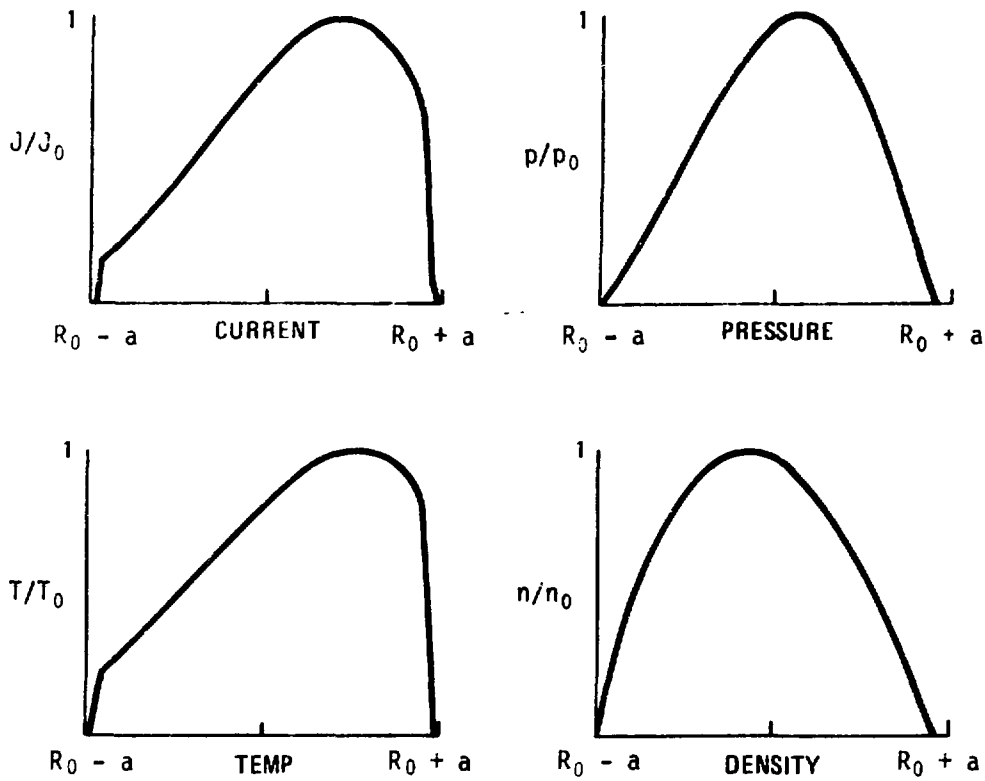

Fig. 5. Distributions of plasma current density, pressure, temperature, and ion density in the GA design.

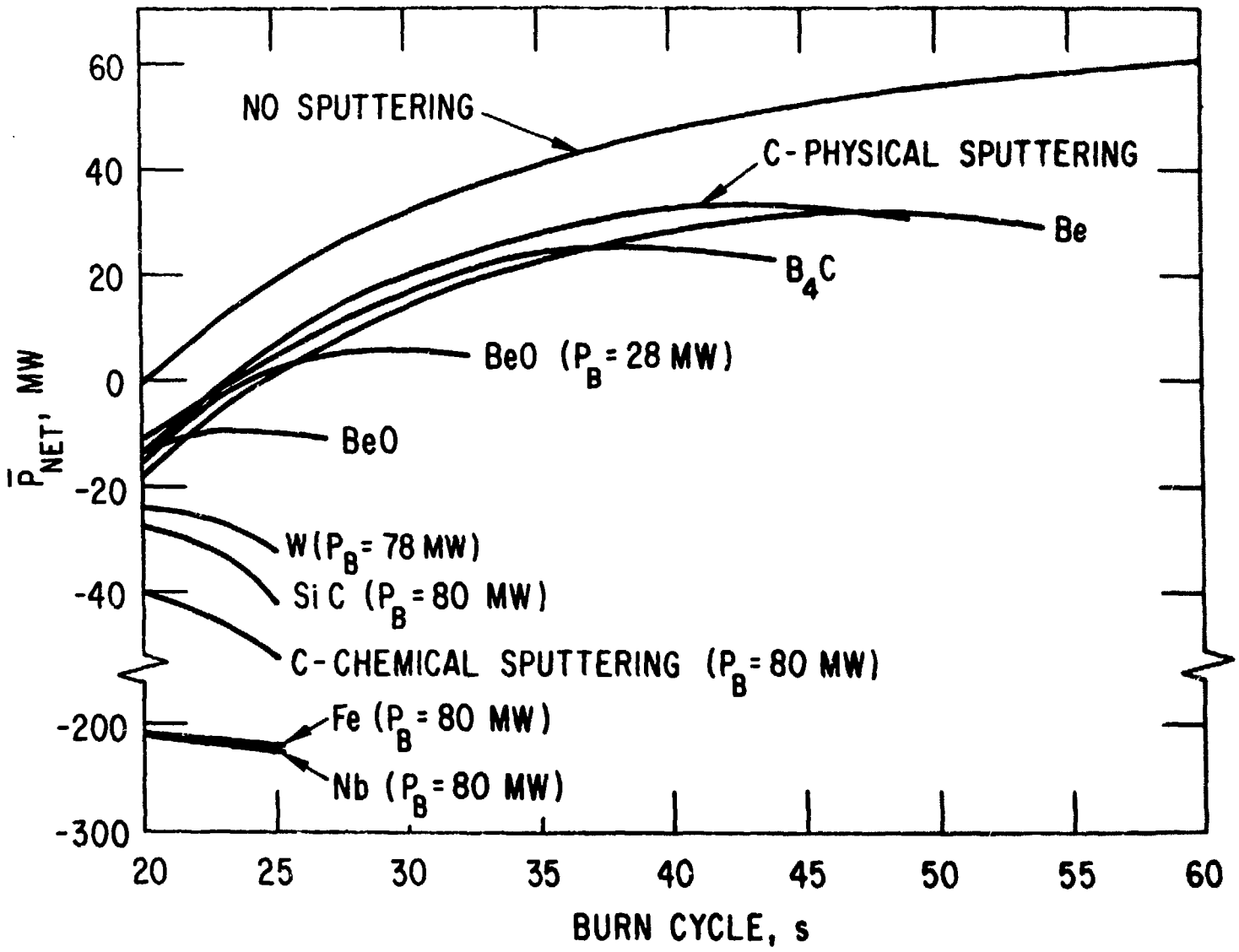

Fig. 6. Effect of first-wall surface material on power performance — ANL design.

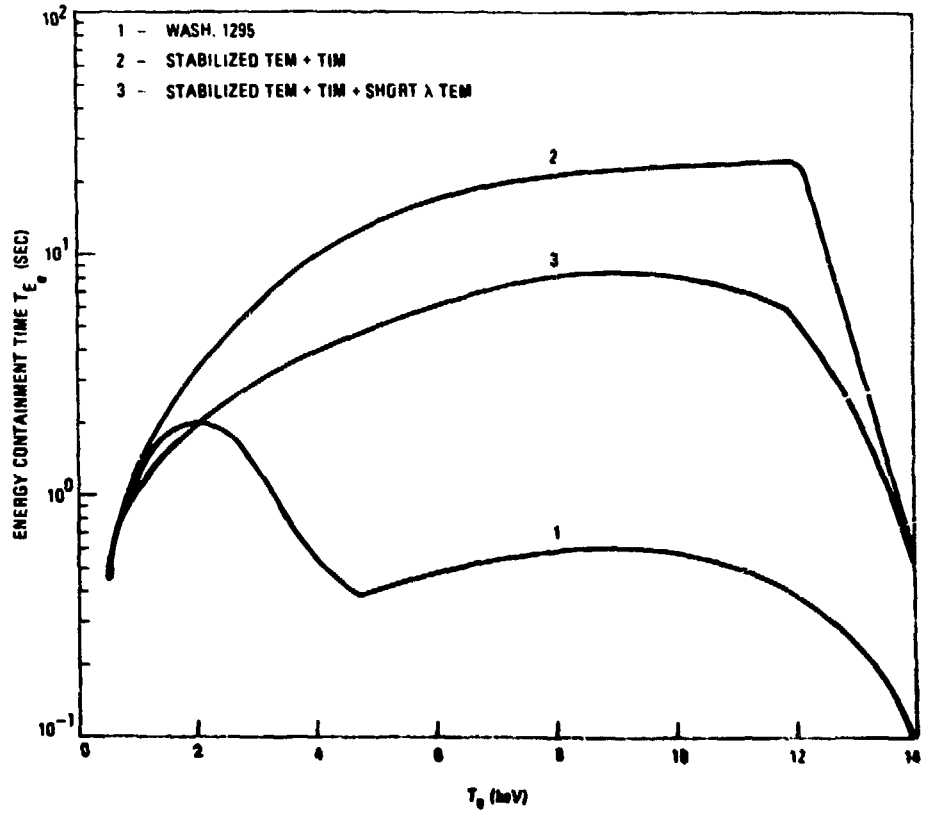

Fig. 7. Energy confinement time as a function of temperature for the GA design.

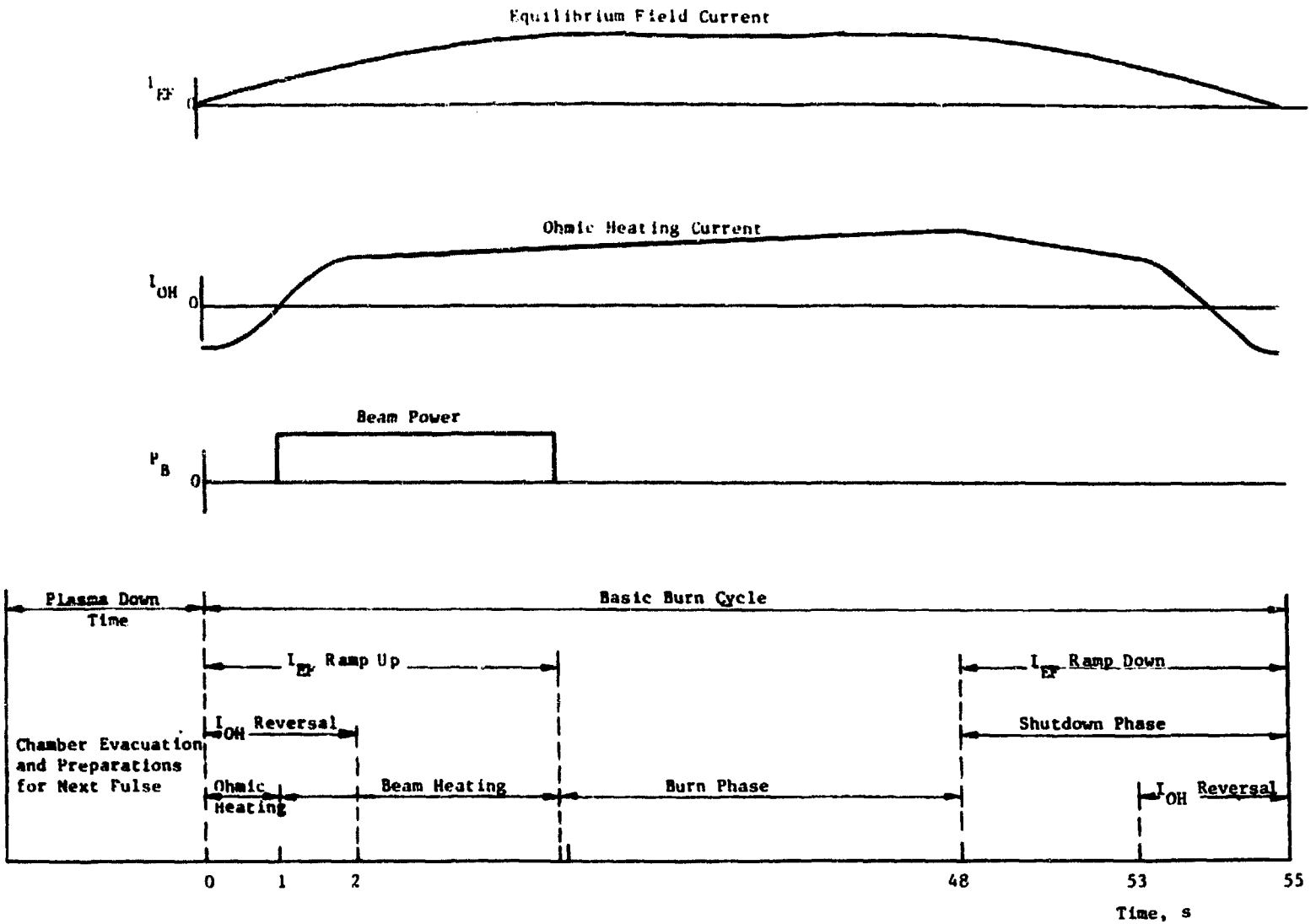

Fig. 8. Burn cycle scenario.

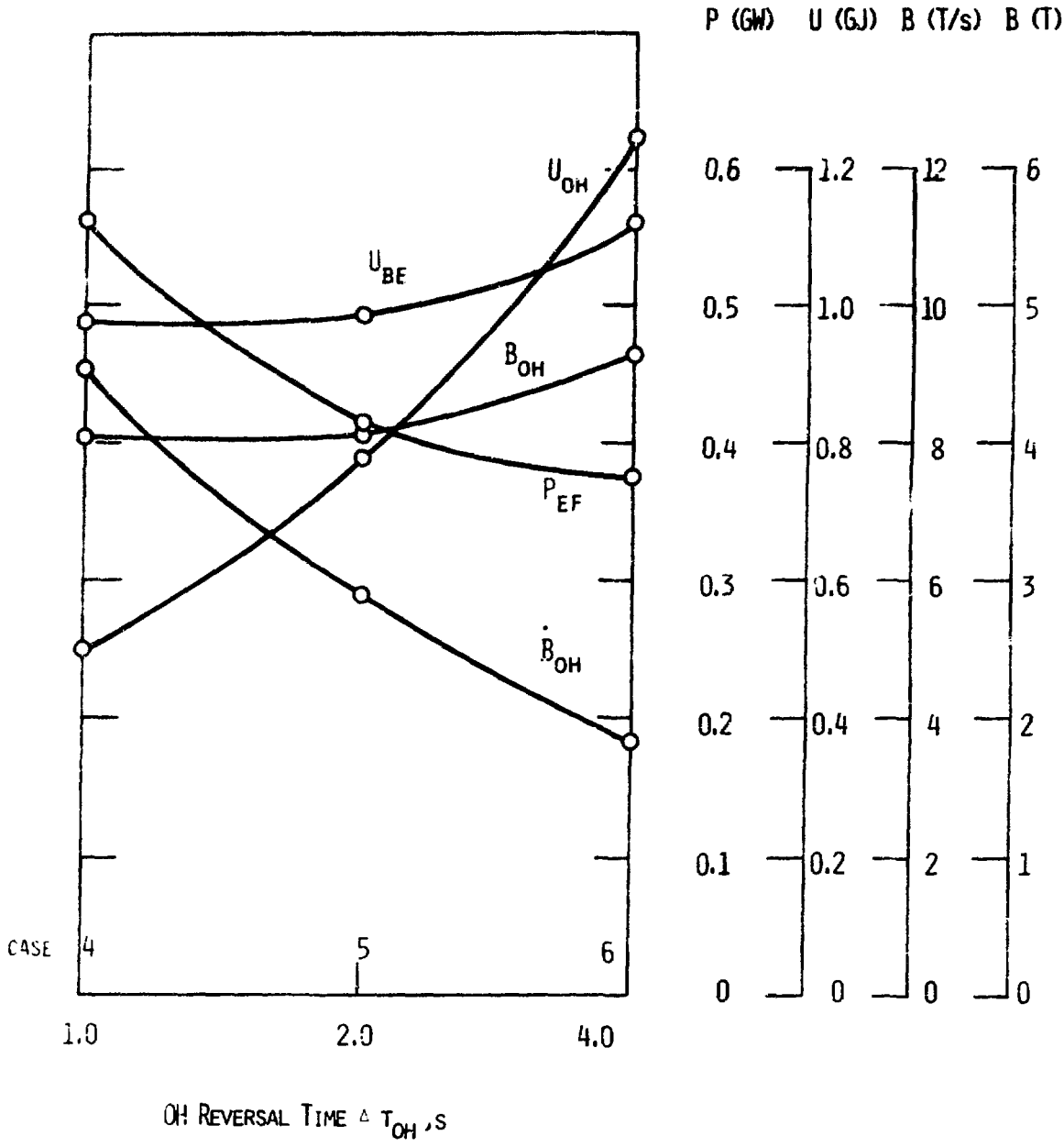

Fig. 9. Effect of OH current reversal time on plasma driving and heating system requirements for the ANL design.

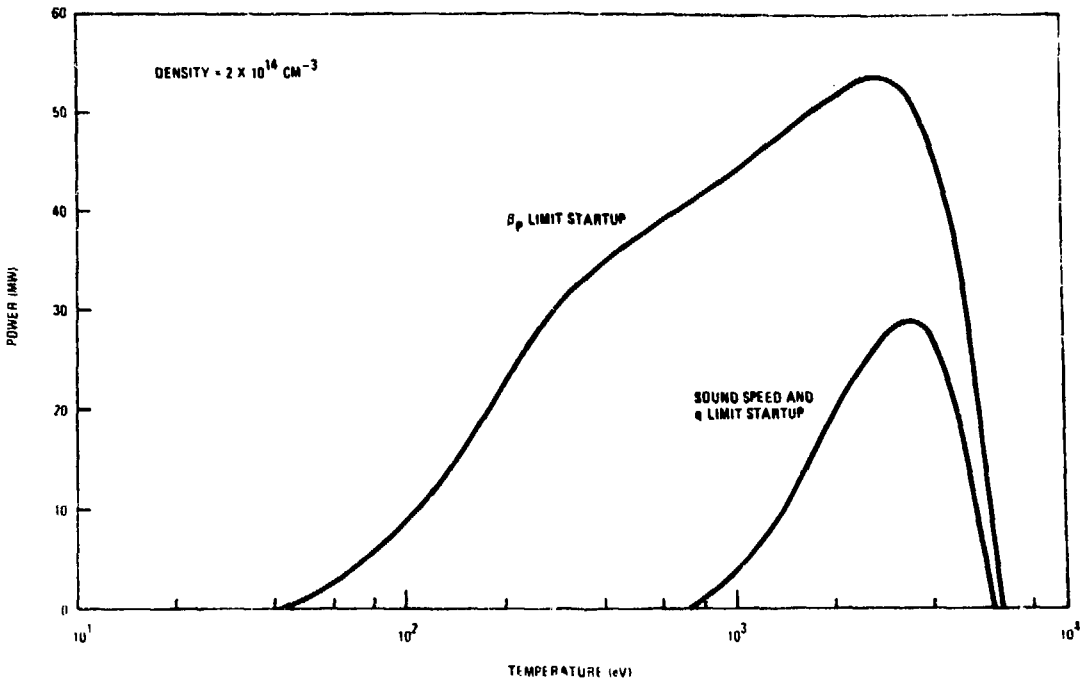

Fig. 10. Auxiliary heating power requirements for the GA design.

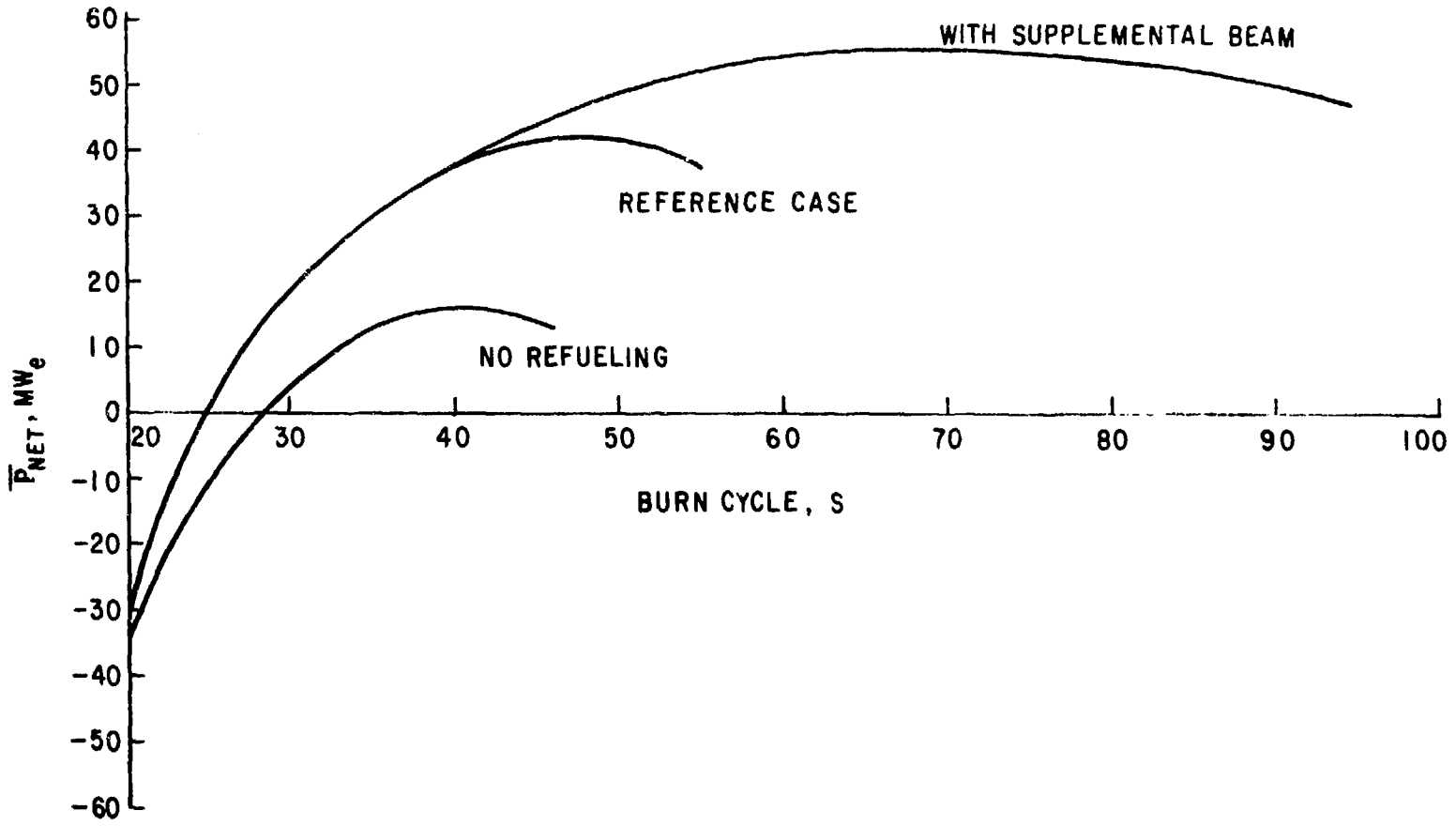

Fig. 11. Power performance as a function of operating mode for the ANL design.